PCCP

Accepted Manuscript

ROYAL SOCIETY OF CHEMISTRY

www.rsc.org/pccp

PCCP: Article

Li^+ Solvation in Glyme-Li Salt Solvate Ionic Liquids

Kazuhide Ueno,[a] Ryoichi Tatara,[a] Seiji Tsuzuki,[b] Soshi Saito,[c] Hiroyuki Doi,[c] Kazuki Yoshida,[a] Toshihiko Mandai,[a] Masaru Matsugami,[d] Yasuhiro Umebayashi,[c] Kaoru Dokko,[a] Masayoshi Watanabe[a]*

[a]Department of Chemistry and Biotechnology, Yokohama National University,79-5 Tokiwadai, Hodogaya-ku, Yokohama 240-8501, Japan

[b]Research Initiative of Computational Sciences (RICS), Nanosystem Research Institute, National Institute of Advanced Industrial Science and Technology (AIST), 1-1-1 Umezono, Tsukuba, Ibaraki 305-8568, Japan

[c]Graduate School of Science and Technology, Niigata University, 8050 Ikarashi, 2-no-cho, Nishi-ku, Niigata City, 950-2181, Japan

[d]Faculty of Liberal Studies, Kumamoto National College of Technology, 2659-2 Suya, Koshi, Kumamoto 861–1102, Japan

K. U. and R. T. equally contributed to this work.

CORRESPONDING AUTHOR FOOTNOTE: To whom correspondence should be addressed.

Telephone/Fax: +81-45-339-3955. E-mail: mwatanab@ynu.ac.jp

ABSTRACT

Certain molten complexes of Li salts and solvents can be regarded as ionic liquids. In this study, the local structure of Li^+ ions in equimolar mixtures ([Li(glyme)]X) of glymes (G3:triglyme and G4: tetraglyme) and Li salts (LiX: lithium bis(trifluoromethanesulfonyl)amide (Li[TFSA]), lithium bis(pentafluoroethenesulfonyl)amide (Li[BETI]), lithium trifluoromethanesulfonate (Li[OTf]), $LiBF_4$, $LiClO_4$, $LiNO_3$, and lithium trifluoroacetate (Li[TFA]) was investigated to discriminate between solvate ionic liquids and concentrated solutions. Raman spectra and ab initio molecular orbital calculations have shown that the glyme molecules adopt a crown-ether like conformation to form a monomeric $[Li_1(glyme)]^+$ in the molten state. Further, Raman spectroscopic analysis allowed us to estimate the fraction of the free glyme in [Li(glyme)]X. The amount of free glyme was estimated to be a few percent in [Li(glyme)]X with perfluorosulfonylamide type anions, and thereby could be regarded as solvate ionic liquids. Other equimolar mixtures of [Li(glyme)]X were found to contain a considerable amount of free glyme, and they were categorized as traditional concentrated solutions. The activity of Li^+ in the glyme-Li salt mixtures was also evaluated by measuring the electrode potential of Li/Li^+ as a function of concentration, by using concentration cells against a reference electrode. At a higher concentration of Li salt, the amount of free glyme diminishes and affects the electrode reaction, leading to a drastic increase in the electrode potential. Unlike conventional electrolytes (dilute and concentrated solutions), the significantly high electrode potential found in the solvate ILs indicates that the solvation of Li^+ by the glyme forms stable and discrete solvate ions ($[Li(glyme)]^+$) in the molten state. This anomalous Li^+ solvation may have a great impact on the electrode reactions in Li batteries.

KEYWORDS: Glyme, Raman spectra, solvate ionic liquids, electrode potential

Table of Contents.

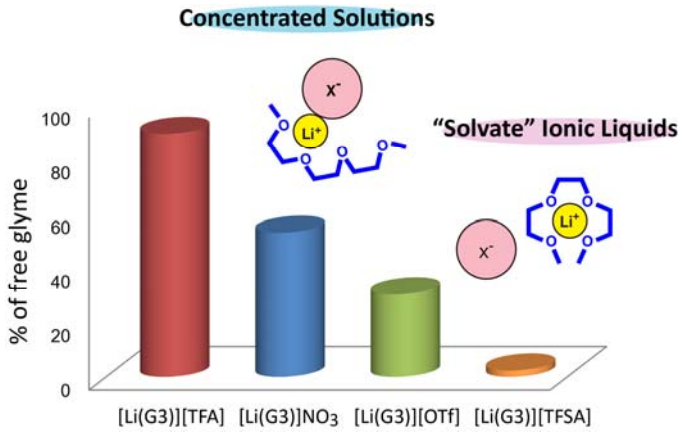

Raman spectra and electrode potentials corroborated that glyme-Li salt solvate ionic liquids consist of crown-ether like complex cation and counter anion with few uncoordinated glyme molecules in the liquid state.

1. Introduction

Non-aqueous electrolytes based on ether solvents afford high solubility of Li salts and chemical stability to lithium metal anodes, enabling their widespread use in lithium primary batteries.[1] Recent developments in lithium ion batteries have resulted in the replacement of these ether solvents by carbonate solvents, because of their incompatibility with graphite anodes and 4V-class cathode materials. However, carbonate electrolytes undergo side reactions with the reaction intermediates of next generation batteries, and hence new alternative electrolytes are required.[2] The growing demand for high energy density batteries such as Li-air and Li-sulfur systems have encouraged researchers to revisit ether-based electrolytes.

Concentrated mixtures of oligo(ethylene glycol) dimethyl ethers (so-called glymes) and Li salts have been a useful model for polyethyleneoxide (PEO)-based polymer electrolytes, in order to study their ionic transport mechanism, correlated with the local coordination structure.[3-6] Stoichiometric mixtures often formed crystalline complexes, and a variety of crystal structures of the solvates with different Li salts and glymes have been determined.[7-9] The glyme-Li salt complexes have also been investigated as small-molecule solid electrolytes.[10, 11] Interestingly, some of these complexes even melt near room temperature.[12]

In recent times, these melts have also attracted attention as lithium conducting liquid electrolytes, as a result of their ionic liquid (IL)-like behavior. This was first pointed out by Pappenfus et al. for equimolar mixtures of tetraglyme (G4) and lithium bis(trifluoromethanesulfonyl)amide (Li[TFSA]) or lithium bis(pentafluoroethenesulfonyl)amide (Li[BETI]),[13] and various IL-like properties such as high thermal stability and low flammability, have since been verified.[14] Moreover, the strong complexation with Li^+ greatly improved the poor electrochemical oxidative stability of the glymes, which in turn allowed the reversible charge-discharge of 4V-class Li-ion batteries.[15] These molten complexes have been termed 'solvate' ILs, and are now recognized as a new generation of ILs in which the ligand molecules (glymes in this study) strongly coordinate as a third species with the cation and/or anion of the salts.[16, 17]

In an earlier work, we reported that low-melting glyme-Li salt equimolar complexes (abbreviated as [Li(glyme)]X) with different Li salts (LiX) and triglyme (G3) or tetraglyme (G4) can be categorized in to two types depending on the counter anion X: ordinal concentrated solutions and solvate ILs.[18] In the former, uncoordinated glyme was found to exist even in the presence of an equivalent amount of the Li salt, while in the latter, 'free' glyme was undetectable, and all the glyme molecules participated in complex formation. This classification of [Li(glyme)]X was based on their physicochemical properties in the molten state. Diffusion measurements by the pulsed field gradient (PFG)-NMR method showed that coupled translational motion of glyme molecules and Li^+ ions can be indicative of the long-lived complex cation $[Li(glyme)]^+$, which is a requirement for solvate ILs.

A crown-ether like conformation of the complex cation $[Li(glyme)]^+$ was suggested for [Li(G3)][TFSA] and [Li(G4)][TFSA], by ab initio molecular orbital calculations.[15] However, the structure of the $[Li(glyme)]^+$ complex has not yet been investigated in detail for [Li(glyme)]X in the melt. Here, we studied the local structure of Li^+ ions in [Li(glyme)]X by Raman spectroscopy, in both liquid and solid states, in order to validate the previous classification of [Li(glyme)]X as a solvate IL. Spectroscopic analysis enabled us to estimate the amount of 'free' glyme in [Li(glyme)]X quasi-quantitatively. Additionally, we show that the electrode potential of Li/Li^+ is strongly influenced by the presence/absence of uncoordinated glyme molecules, as well as activity of Li^+ (or $[Li(glyme)]^+$) cation in the electrolyte.

2. EXPERIMENTAL SECTION

Materials. Purified glymes (water content < 50 ppm), triglyme (G3) and tetraglyme (G4), were kindly supplied by Nippon Nyukazai Co., Ltd., and Li[TFSA] (battery-grade, water content < 50 ppm) was obtained, courtesy of Solvay Chemicals. Battery-grade Li salts, Li[BETI], lithium trifluoromethanesulfonate (Li[OTf]), $LiBF_4$, and $LiClO_4$, from Kishida Chemical Co., Ltd., were used as received. The other Li salts, $LiNO_3$, lithium trifluoroacetate (Li[TFA]), and $LiAsF_6$ (from Sigma-Aldrich), were dried under high vacuum at an elevated temperature prior to use. Equimolar glyme-Li salt mixtures

were prepared by mixing appropriate amounts of the lithium salt and glyme in an Ar-filled glove box (VAC, [H_2O] < 1 ppm). Typically, the lithium salt and glyme were mixed and magnetically stirred in a vial, at 60 °C overnight. When necessary, the samples were further heated above their melting point for several hours to ensure complete mixing. In this study, the glyme–LiX mixtures at 1:1 molar ratios are referred to as [Li(glyme)]X (indicating the pair of $[Li(glyme)]^+$ cation and X^- anion), and does not necessarily correspond to the actual chemical formulation in the molten state, whereas, it represents the intended formula for the crystalline complexes. Because of low thermal stability of the Li salt, [Li(G4)]AsF_6 was prepared by mixing equimolar amounts of G4 and $LiAsF_6$ in an acetonitrile solution, followed by removal of the solvent under vacuum.

Measurements. The densities of the mixtures were measured by the SVM3000 viscometer (Anton Paar), and the molar concentration of Li salt was calculated from the solution density. Raman spectra of the samples were recorded using a 532 nm laser Raman spectrometer (NRS-4100, JASCO), which was calibrated using polypropylene and polystyrene standards. The samples were sealed in a capillary tube, and their temperature was adjusted to 30 ± 0.1 °C (unless stated otherwise) using a Peltier microscope stage (TS62, INSTEC) with a temperature controller (mk1000, INSTEC). Raman bands were analyzed using the JASCO spectra manager program. When necessary, the intensity was normalized with respect to the Raman band at 1400–1550 cm^{-1} (assigned to CH_2 bending/scissoring mode),[19] on the basis of the concentration of glyme in the mixtures. The normalized spectra were deconvoluted by a Gaussian-Lorentzian function for spectroscopic analysis.

Ionic conductivity was measured by the complex impedance method, in the frequency range of 500 kHz–1 Hz with 100 mV amplitude (VMP3, Bio-Logic). Two platinum black electrodes (CG-511B, TOA Electronics, cell constant ≈ 1 cm^{-1}) were dipped in the mixture, and the sample cell was thermally equilibrated at each temperature for at least 30 min using a thermostat chamber.

The electrode potentials of Li/Li^+ for the sample electrolytes were measured by recording the potential difference of a concentration cell between two Li metal specimens in the sample electrolytes,

and in the reference electrode (Li/Li^+ in 1 mol dm^{-3} Li[TFSA]/G3). Vycor glass was used for the junction between the reference electrolyte and the sample electrolytes. The potential was recorded using a VMP3 multi-potentiostat (Bio-Logic) at 30 °C in a thermostat chamber. Because the transference number of Li^+ is approximately 0.5 in the glyme-Li salt mixtures,[18, 20] the effect of junction potential was assumed to be negligible in this experiment.

High-energy X-ray diffraction (HEXRD) measurements were carried out at 298 K, using the BL04B2 beam-line of SPring-8 at the Japan Synchrotron Radiation Research Institute (JASRI).[21, 22] The sample solvate IL was set in a cell made of 2 mm thick polyetheretherketone plates, with Kapton® films as an X-ray window, hermetically sealed with Kalrez® O rings, and stainless steel cover plates. Monochrome 61.6 keV X-rays were obtained using a Si (220) monochromator. The observed X-ray intensity was corrected for absorption[23] and polarization. Incoherent scatterings[24] were subtracted to obtain coherent scatterings, $I_{coh}(Q)$, where Q represents a scattering vector $Q = 4\pi\sin\theta/\lambda$ (θ and λ stand for the scattering angle, and the wavelength of the X-ray, respectively). The X-ray structure factor $S(Q)$ per stoichiometric volume was obtained, according to

$$S(Q) = \frac{I_{coh}(Q) - \sum n_i f_i(Q)^2}{(\sum n_i f_i(Q))^2} + 1 \qquad (1)$$

where n_i and $f_i(Q)$ denote the number and the atomic scattering factor of atom i,[25] respectively. All data analysis was carried out using the program KURVLR.[26]

Computational methods. The Gaussian 09 program was used for density functional theory (DFT) calculations.[27] The basis sets implemented in the Gaussian program were used, and the geometries of complexes were fully optimized at the B3LYP/6-311+G** level. Calculations were carried out at the same level for vibrational analysis.

3. RESULTS AND DISCUSSION

Coordination structure. Several crystalline solvates of equimolar glyme–Li salt mixtures, [Li(G3)]X or [Li(G4)]X, have been reported by Henderson and coworkers.[7-9] Their single crystal X-ray diffraction studies have shown that the coordination structure of the complexes strongly depends on the glyme and the counter anion X. [Li(G3)][OTf] forms arrays of helical chains of G3 molecules cross-linked by Li^+ ions; each G3 molecule is associated with 2 Li^+ cations. Li^+ ions adopt a 5-fold coordination, and are bonded to 1 oxygen atom from the $[OTf]^-$ anion, and 4 oxygens from two G3 molecules. The same lithium coordination environment was seen in other 1:1 complexes, such as crystalline [Li(G3)]ClO_4, [Li(G3)]BF_4, and [Li(G3)]AsF_6.[7] In contrast to these complexes with a polymeric coordination ($[Li_n(G3)_n]^{n+}$), the [Li(G3)][BETI] crystal consists of a monomeric $[Li(G3)]^+$ cation adopting a crown-ether (12-crown-4) like conformation, and a $[BETI]^-$ anion. In this complex, Li^+ is coordinated to four oxygen atoms from a single G3 molecule and one oxygen atom from the $[BETI]^-$ anion.[9] Very recently, the crystal structure of the low-melting [Li(G3)][TFSA] was reported[28] as having a similar coordination structure to [Li(G3)][BETI], with monomeric $[Li(G3)]^+$ cations. However, Li^+ is 6-fold coordinated, with four oxygen atoms from a single G3 molecule and two oxygen atoms from a single $[TFSA]^-$ anion. For G4-based crystalline complexes, a double helix dimer composed of two Li^+ cations and two G4 molecules ($[Li_2(G4)_2]^{2+}$) has been found in [Li(G4)]AsF_6.[8] Each Li^+ is coordinated to three oxygen atoms from each G4 molecule (6-fold coordination), and the central oxygen atom of each G4 molecule coordinates to both Li^+ cations. The AsF_6^- anion does not participate in coordination.

Raman spectroscopy is a powerful technique for characterization of the coordination structures of equimolar complexes, in solid and liquid state. For glymes, the Raman bands between 800 and 900 cm^{-1} have been assigned to a mixture of modes for CH_2 rocking vibrations and C-O-C stretching vibrations.[29-31] It is known that a prominent band appears at 865–890 cm^{-1} upon complex formation with metal ions (the so-called breathing mode).[29, 32, 33] Therefore, the Raman spectrum in this region reflects the coordination structure of the glyme-Li salt complexes. Raman spectra of the pure glymes and equimolar mixtures of [Li(G3)]X and [Li(G4)]X are shown in **Figure 1**. Pure G3 and G4 showed very similar Raman spectra with three bands at 809, 828, and 851 cm^{-1}, with no visible bands in the range of 865–890 cm^{-1}.

These bands were attributed to the vibrations of different conformational sequences of the ethylene oxide chains with *trans* (*t*), *gauche plus* (*g*), and *gauche minus* (*g′*) arrangements. In this study, we did not focus on the detailed assignments of the bands to the different conformations because of their complexity.[34, 35] To determine the coordination structure of [Li(glyme)]X in the liquid state, the spectra were simply compared to those in the solid state for which the single crystal structure is known.

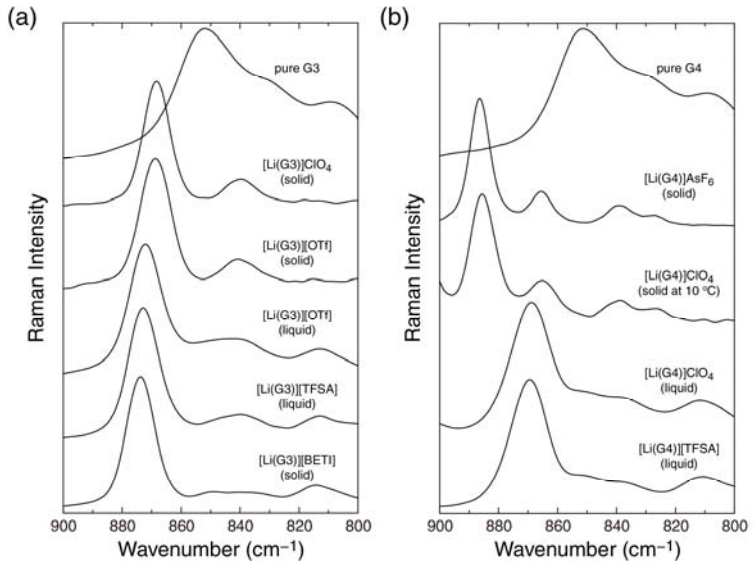

Figure 1. Raman spectra of (a) $[Li(G3)_1]X$ and pure G3 and (b) $[Li(G4)_1]X$ and pure G4 in the frequency range 800–900 cm^{-1}.

The spectra of solid $[Li(G3)]ClO_4$ and [Li(G3)][OTf] are quite similar (**Figure 1a**) with two bands at 840 and 868 cm^{-1}, consistent with their identical structure possessing the helical $(tg't)_3$ conformation.[7] Because the low-melting [Li(G3)][OTf] forms a relatively stable, supercooled liquid at 30 °C, we also obtained the Raman spectrum of [Li(G3)][OTf] in the liquid state at the same temperature. As seen in **Figure 1a** the spectral shape of [Li(G3)][OTf] changed upon melting, with the breathing mode shifting slightly to a higher frequency and the appearance of a new band at 813 cm^{-1}. These changes are indicative of different coordination structures of $[Li(G3)]^+$ in the solid and liquid states. Raman spectra of another crystalline complex [Li(G3)][BETI], and the liquid equimolar mixture [Li(G3)][TFSA] are also shown in **Figure 1a** for comparison. The solid [Li(G3)][BETI] exhibits a very strong band at 873 cm^{-1}, which was

assigned to the breathing mode, along with weaker bands at 814, 838, and 850 cm^{-1}. The spectra of liquid [Li(G3)][TFSA] and [Li(G3)][OTf] appear very similar to the solid [Li(G3)][BETI]. In addition, the spectrum of [Li(G3)][OTf] is somewhat broader than the other mixtures, possibly due to a superposition of the spectra of pure G3 and [Li(G3)][BETI]. This raises the possibility that a certain amount of G3 remains uncoordinated even in the equimolar mixture, [Li(G3)][OTf] melt.

Raman spectra of equimolar mixtures of [Li(G4)]X and pure G4 are shown in **Figure 1b**. Solid [Li(G4)]AsF_6 and [Li(G4)]ClO_4 exhibit four bands at 823, 839, 865, and 886 cm^{-1}. The intense band at 886 cm^{-1} was assigned to the *tgt-tg′t* sequence of the double helix dimer $[Li_2(G4)_2]^{2+}$.[32] In liquid [Li(G4)]ClO_4 and [Li(G4)][TFSA], there is no band at 886 cm^{-1}, indicating the absence of the *tgt-tg′t* sequence in the liquid state. The spectra of these liquids were characterized by the four bands at 812, 835, 850, and 870 cm^{-1}. Because only the double helix dimer $[Li_2(G4)_2]^{2+}$ has been reported for crystalline [Li(G4)]X,[8] Raman bands of other possible structures such as a crown-ether like $[Li(G4)]^+$ were studied by DFT calculations.[36, 37]

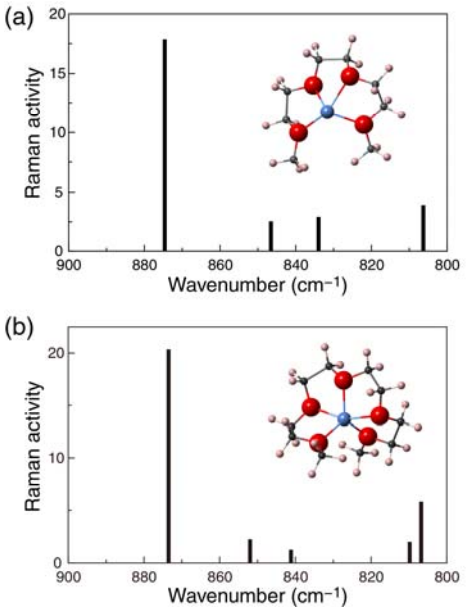

Figure 2. The calculated Raman bands and the corresponding optimized geometries of (a) $[Li(G3)]^+$ and (b) $[Li(G4)]^+$ at the B3LYP/6-311+G** level.

The HF/6-311G** level optimized geometries for $[Li(G3)]^+$ ions[15] and $[Li(G4)]^+$ ions,[37] were used to obtain initial geometries for the B3LYP/6-311+G** level geometry optimizations and vibrational analysis. **Figure 2** displays the optimized geometries and predicted Raman bands for the $[Li(G3)]^+$ and $[Li(G4)]^+$ cations. We confirmed that the calculated Raman spectrum of $[Li(G3)]^+$ had an intense band at 874 cm^{-1} associated with weaker bands at 806, 833, and 846 cm^{-1} (**Figure 2a**). These bands are quite similar to those for experimental Raman bands of solid [Li(G3)][BETI] and liquid [Li(G3)]X with $[TFSA]^-$ and $[OTf]^-$. Therefore, we can conclude that the G3 molecules adopt a crown-ether like conformation to form a monomeric $[Li(G3)]^+$ in these liquid mixtures. The predicted bands of $[Li(G4)]^+$ can be seen at 807, 810, 841, 851, and 873 cm^{-1} (**Figure 2b**). The resemblance between the experimental Raman bands of the liquid [Li(G4)]X and the calculated Raman bands for $[Li(G4)]^+$ suggests that the G4 molecule is wrapped around the Li^+ in a manner similar to the optimized geometry (**Figure 2b** inset) in the liquid state.

Compared to the polymeric and dimeric coordination structures found in the crystalline phases of [Li(G3)]X and [Li(G4)]X, the monomeric form of $[Li(glyme)]^+$ would be energetically favorable in the liquid state, due to a larger gain in the translational and rotational entropies. As a result, the complex cations likely exist as the crown-ether-like monomeric $[Li(glyme)]^+$ in the liquid state.

Concentration dependence of Raman spectra. Solvation of Li^+ ions in the equimolar mixtures [Li(glyme)]X is governed by competitive cation-anion and cation-solvent interactions. Therefore, one may expect that a certain amount of the glyme remains uncoordinated in [Li(glyme)]X with an associative Li salt, according to a simple equilibrium: $LiX + glyme \rightleftarrows [Li(glyme)]^+ + X^-$. This was indeed suggested by our previous classification of [Li(glyme)]X into solvate ILs and the concentrated solutions, based on the diffusion measurements using PFG-NMR.[18] The ratio of self-diffusion coefficients of glyme and lithium (D_G/D_{Li}) was clearly higher than unity for the concentrated solutions ([Li(glyme)]X with a less dissociative LiX). This was attributed to either a fast ligand exchange between the unstable $[Li(glyme)]^+$ cations, or the presence of free glymes that do not participate in the coordination of Li^+ ions. In contrast,

D_G/D_{Li} was almost unity in solvate ILs ([Li(glyme)]X with a more dissociative LiX) suggesting the presence of the long-lived $[Li(glyme)]^+$.

The difference in the amount of free glyme in [Li(glyme)]X can also be seen in the Raman spectra normalized by the total concentration of glyme. **Figures 3 a and b** show the normalized Raman spectra of equimolar mixtures of [Li(G3)]X and G3-Li[BETI] mixtures with different molar fractions of Li[BETI] ($X_{Li[BETI]}$) in the range of 800–900 cm^{-1}, respectively. In **Figure 3a**, the spectral shape strongly depends on the structure of the anion X. The spectra of [Li(G3)]X with an associative Li salt such as Li[OTf], $LiNO_3$, and Li[TFA], showed a lower intensity for the breathing mode at ~873 cm^{-1}, and the higher intensity of the bands in the range of 800–850 cm^{-1}, compared to those for the solid [Li(G3)][BETI] in which no free glyme exists. The change in the intensities of the bands of [Li(G3)]X appears to resemble the spectral changes of the mixture of G3-Li[BETI] in **Figure 3b**. Upon the addition of excess glyme to solid [Li(G3)][BETI], the intensity of the breathing mode at 873 cm^{-1} decreases significantly, whereas the three bands at 809, 828, and 851 cm^{-1} increase, accompanied by a small frequency shift. Therefore, the presence of free G3 could be responsible for the lower intensity of the breathing mode and the higher intensities of the bands in the range of 800–850 cm^{-1}.

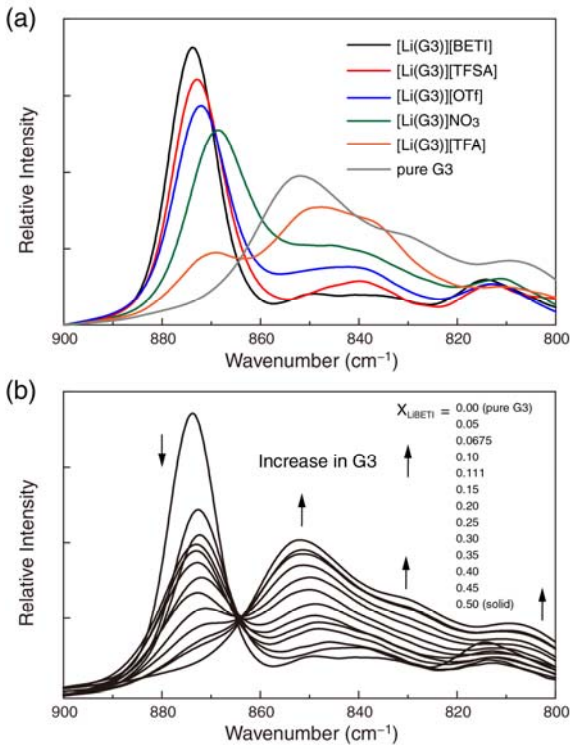

Figure 3. Normalized Raman spectra of (a) [Li(G3)]X and (b) G3-Li[BETI] mixtures with different molar ratios of Li[BETI] (X_{LiBETI}).

In order to further elucidate the Li^+ ion species in [Li(glyme)]X, concentration dependent Raman spectra of the G3-Li[BETI] mixtures (**Figure 3b**) were analyzed as model systems. Herein, the Raman spectra were deconvoluted into four bands at around 810, 835, 850, and 873 cm^{-1}, by a Gaussian-Lorentzian function. Typical results are shown in the Supplementary Information (**Figure S1)**. Concentration dependent Raman spectra of [Li(glyme)]X, and other G3-LiX and G4-LiX mixtures (**Figure S2**) were also similarly analyzed.

Although the bands of the solid [Li(G3)][BETI] overlap with the three bands of pure G3 at 809, 828, and 851 cm^{-1}, the change in the intensities of the bands in the range of 800–850 cm^{-1} can be ascribed to the change in the concentration of the free G3 molecules associated with complex formation. Here, we assumed the sum of the integral intensities of the three bands, I_{850}, I_{835}, and I_{810}, to be the integral intensity of the uncoordinated G3 band, I_f, in the dilute region of Li[BETI] (i.e. $I_f = I_{850} + I_{835} + I_{810}$). I_f is related to the concentration of free G3 (c_f) in the mixtures: $I_f = J_f c_f$, where J_f is the molar Raman scattering

coefficient of free G3 molecules in this frequency range. Because $c_f = c_G - nc_{Li}$,[38] where n denotes the solvation number of the Li^+ ion, we obtain the following relationship;

$$I_f/c_{Li} = J_f(c_G/c_{Li} - n) \qquad (2)$$

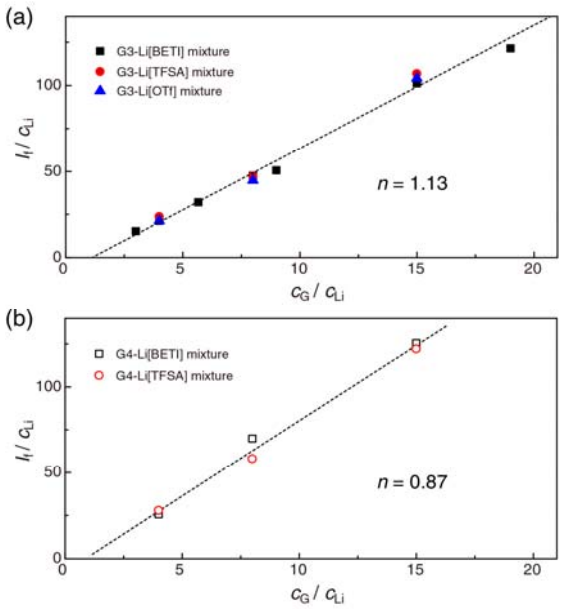

Figure 4. Plots of I_f/c_{Li} against c_G/c_{Li} for the bands in the range of 800−850 cm^{-1} of (a) G3-LiX mixtures and (b) G4-LiX mixtures in the dilute region. The broken lines represent the best linear fitting by the equation $I_f/c_{Li} = J_f(c_G/c_{Li}-n)$.

In **Figure 4**, I_f/c_{Li} was plotted against c_G/c_{Li} for G3-LiX and G4-LiX mixtures in the dilute region. The plots yield a straight line, and J_f and n can be obtained from the slope and the intercept, respectively. The n values for the mixtures are ~1, indicating that both G3 and G4 form a complex cation with Li^+ at 1:1 molar ratio in the dilute solution. In the concentrated region, the bands in the range of 800–850 cm^{-1} could not be assigned to free G3 molecules because of the non-negligible band overlap. Nonetheless, the solvation number n is also probably one in the concentrated mixtures on the basis of the reported crystal structures and their Raman spectra, as discussed in the previous section.

Because the band at 873 cm^{-1} was enhanced with increasing c_{Li}, we expected that the linear relationship between I_{873} and c_{Li} also holds as $I_{873} = J_b nc_{Li}$ with the scattering coefficient of the bound

glymes (J_b). However, the plot of I_{873} versus c_{Li} had an intercept unlike the expected relationship (data not shown). This suggests that vibrations of free G3 molecules also contribute in part to the band at 873 cm^{-1}. Thus I_{873} can be represented by contribution from both free (I_{f873}) and bound (I_{b873}) glymes as

$$I_{873} = I_{f873} + I_{b873} = J_{f873}c_f + J_{b873}c_b \qquad (3)$$

where c_b, J_{f873} and J_{b873} represent the concentration of bound G3 to Li^+ ions, and the molar Raman scattering coefficients of the free and bound G3 for the band at ~873 cm^{-1}, respectively. In dilute solutions, from the relations $c_b = nc_{Li}$, $c_f = c_G - nc_{Li}$ and $n \sim 1$, we obtained the relation between I_{873}, c_G and c_{Li} as follows:

$$I_{873}/c_G = J_{f873} + (J_{b873} - J_{f873})c_{Li}/c_G \qquad (4)$$

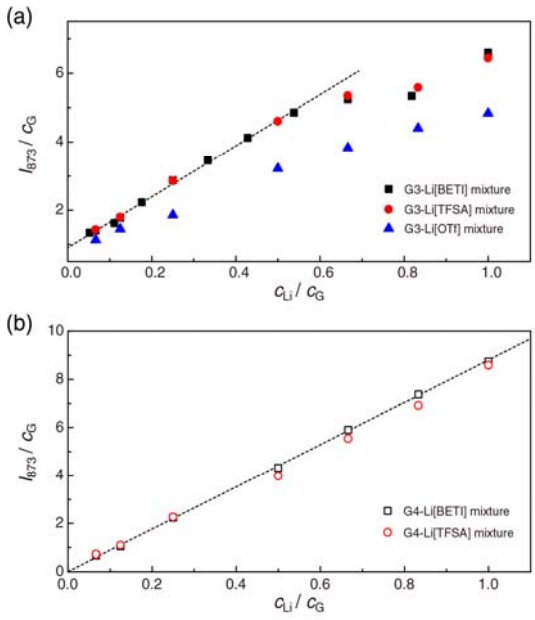

Figure 5. Plots of I_{873}/c_G against c_{Li}/c_G for the bands at ~873 cm^{-1} of (a) G3-LiX mixtures and (b) G4-LiX mixtures. The dotted lines represent the best linear fit by the equation $I_{873}/c_G = J_{f873} + (J_{b873} - J_{f873})c_{Li}/c_G$ for the data of G3-Li[BETI] and G4-Li[BETI] mixtures.

As can be seen in **Figure 5**, the plot has a linear relationship in the dilute region, and J_{f873} and J_{b873} can be estimated from the slope and the intercept, according to Eq. 3. In **Figure 5a**, the values of I_{873}/c_G are lower for the G3-Li[OTf] mixtures, and level off at higher c_{Li}/c_G for the G3-Li[BETI] and G3-Li[TFSA] mixtures. This is either due to the generation of free glymes, or the simple decrease in the value of Raman scattering coefficient of $[Li(glyme)_1]^+$ (J_{b873}). Although we could not clarify which factor is predominant, both are attributed to the pronounced cation-anion (Li-X) interactions. Here we assume that J_{f873} and J_{b873} obtained from the most dissociative G3-Li[BETI] and G4-Li[BETI] mixtures in the dilute region are constant, independent of the composition of the mixture, and they reflect the ideal J_{f873} and J_{b873} of pure G3 and $[Li_1(G3)_1]^+$, respectively, without any contribution from the counter anion. We can then estimate c_f in the equimolar 1:1 mixture $Li[(glyme)_1]X$, by replacing c_b with $c_G - c_f$ in Eq. 2:

$$c_f = \left(I_{873} - J_{b873}c_G\right)/\left(J_{f873} - J_{b873}\right) \qquad (5)$$

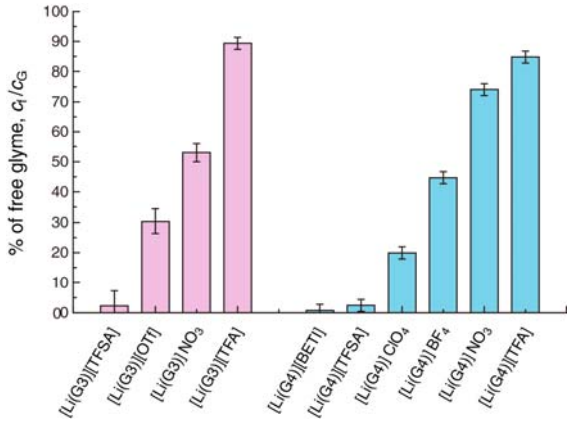

Figure 6. Estimated percentages of free glyme (c_f/c_G) in equimolar molten mixtures $[Li(glyme)_1]X$ at 30 °C.

Figure 6 illustrates the estimated fraction of uncoordinated glyme molecules (c_f/c_G) in [Li(glyme)]X. The percentage of free glyme increases with increasing cation-anion (Li-X) interactions characterized by Lewis basicity (or an electron-pair donating ability) of the anions,[39] and/or calculated Li-X ion-pair dissociation energies:[40] [BETI] < [TFSA] < ClO_4 < BF_4 < [OTf] < NO_3 < [TFA]. The fraction of free glyme was found to be only a few percent in [Li(glyme)]X with [TFSA] and [BETI] anions, confirming that they

mostly consist of the complex cation $[Li(glyme)]^+$ and the counter anions. Therefore, they can be deemed as solvate ILs. The other equimolar mixtures of [Li(glyme)]X contain non-negligible amounts of free glymes (>10 %), and should be categorized as ordinary concentrated solutions or poor solvate ILs.[17] These results are generally consistent with the previous classification of [Li(glyme)]X into the two categories based on their diffusivity ratios (D_G/D_{Li}). Indeed, we could confirm that there is a good correlation between the percentage of free glymes determined by Raman spectra, and the D_G/D_{Li} obtained from the dynamic properties in the NMR time scale of ~10 ms (**Figure 7**). In a previous report, $[Li(G4)]ClO_4$ was regarded as a solvate IL from its D_G/D_{Li} value of 1.06. However, $[Li(G4)]ClO_4$ was found to contain ~20 % of free glyme from Raman spectroscopic analysis, and it should be categorized as a concentrated solution or a poor solvate IL.

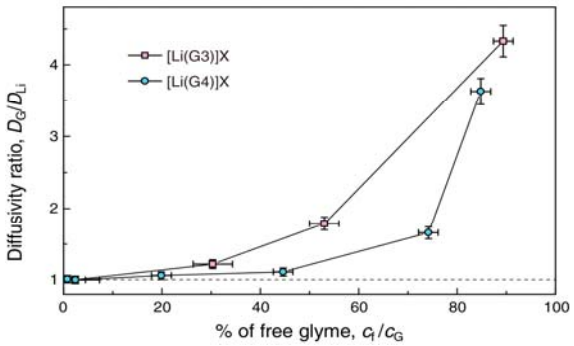

Figure 7. Plots of the diffusivity ratio against the estimated fraction of free glyme (c_f/c_G) in [Li(glyme)]X. The diffusivity ratio data were obtained from ref. 18. The horizontal dotted line indicates $D_G/G_{Li} = 1$.

HEXRD measurements.

The local structure of Li^+ in some solvate ILs was further studied by HEXRD measurements. **Figure 8a** shows the experimental X-ray structure factors for [Li(G3)][TFSA] and [Li(G4)][TFSA] at $Q < 3.0$ $Å^{-1}$. Two intense peaks that are characteristic of the [TFSA]-based ILs[40] were observed at ~0.8 and 1.5 $Å^{-1}$ for both solvate ILs. Additionally, the X-ray structure factors for the two solvate ILs clearly differ from each other, suggesting that the local structure of Li^+ and/or its long range ordering are noticeably different. From the figure it is clear that both peak positions for [Li(G3)][TFSA] are slightly smaller than those for

[Li(G4)][TFSA], indicating that larger Li-solvated clusters exists in the former. In addition, these two peaks have higher intensities for [Li(G3)][TFSA] than [Li(G4)][TFSA], suggesting that more of the larger Li-solvate clusters exist in [Li(G3)][TFSA], and the experimental values of $S(Q)$ indicate that the formation of contact ion-pairs (CIPs) (such as [Li(glyme)][TFSA] and/or $[Li(TFSA)_2]^-$) is greater in [Li(G3)][TFSA]. Though the discussion is rather speculative, greater CIP formation in [Li(G3)][TFSA] is consistent with the Raman results.[29] MD simulations based on the improved force fields qualitatively reproduced the experimental $S(Q)$ as shown by **Figure 8b**. A more detailed analysis of the MD simulations, such as pair distribution functions and coordination numbers, has been discussed elsewhere.[41] MD simulations have shown that Li^+ was coordinated by all four oxygen atoms from G3 and one oxygen atom from $[TFSA]^-$ in [Li(G3)][TFSA]. On the other hand, the coordination number of oxygen atoms of G4 was about 4.5 and that of $[TFSA]^-$ was 0.5 in [Li(G4)][TFSA]. This suggests greater CIP formation in [Li(G3)][TFSA] than [Li(G4)][TFSA], which agrees with the interpretation of the experimental data.

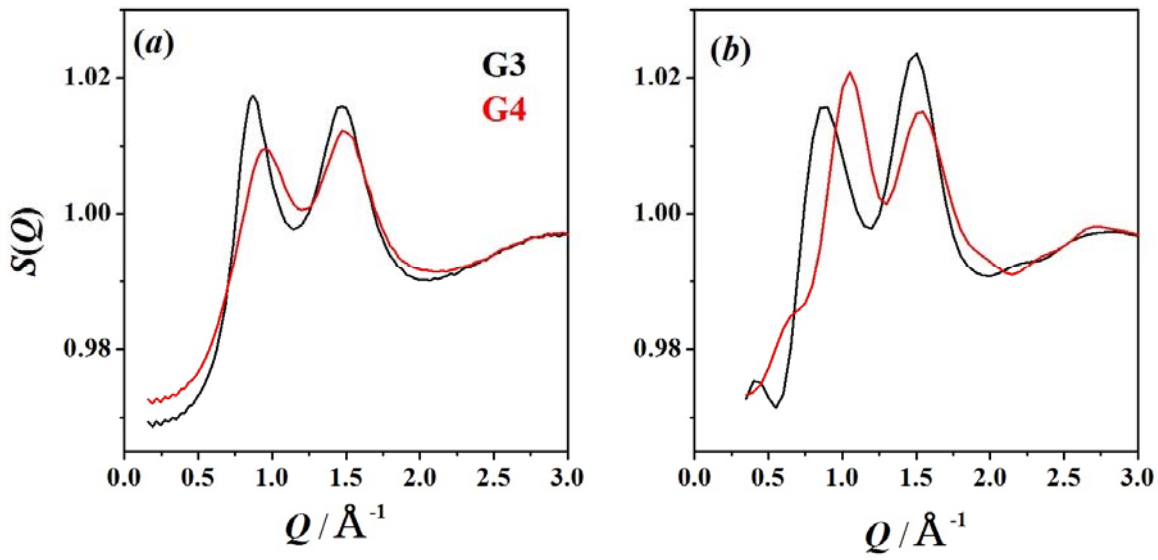

Figure 8 Experimental (*a*) and simulated (*b*) X-ray structure factors for the LiTFSA-G3 (black) and LiTFSA-G4 (red) 1:1 solvated ionic liquids. Simulated one was evaluated from MD trajectories at 303 K.

Electrode potential.

The activity (or activity coefficient) of solvated ions has been studied for electrolyte solutions, and are strongly dependent upon the ion solvation environment.[42] According to the equilibrium reaction, $Li^+ + e^- \rightleftarrows Li$, the electrode potential of Li metal (E_l) is associated with the activity of Li^+ (a_{Li+}) by the Nernst equation:

$$E_l = E_l^0 + \frac{2.303RT}{F}\log a_{Li^+} \quad (6)$$

where E_l^0 is the standard electrode potential, R is the gas constant, T is the absolute temperature, and F is the Faraday constant. In this respect, elucidation of the electrode potential of Li/Li^+ in highly concentrated [Li(glyme)]X is of great interest. Similar to a previous report,[43] we found that the electrode potential in the G3-Li[TFSA] mixtures increases drastically in the region of high concentration (c_{Li} > 1 mol dm^{-3}), and was ~200 mV higher in the equimolar composition of [Li(G3)][TFSA] with respect to the reference electrode (Li/Li^+ in 1 mol dm^{-3} Li[TFSA]/G3). **Figure 9** shows the concentration dependence of the electrode potential in the glyme-LiX mixtures with different anionic structures at 30 °C.

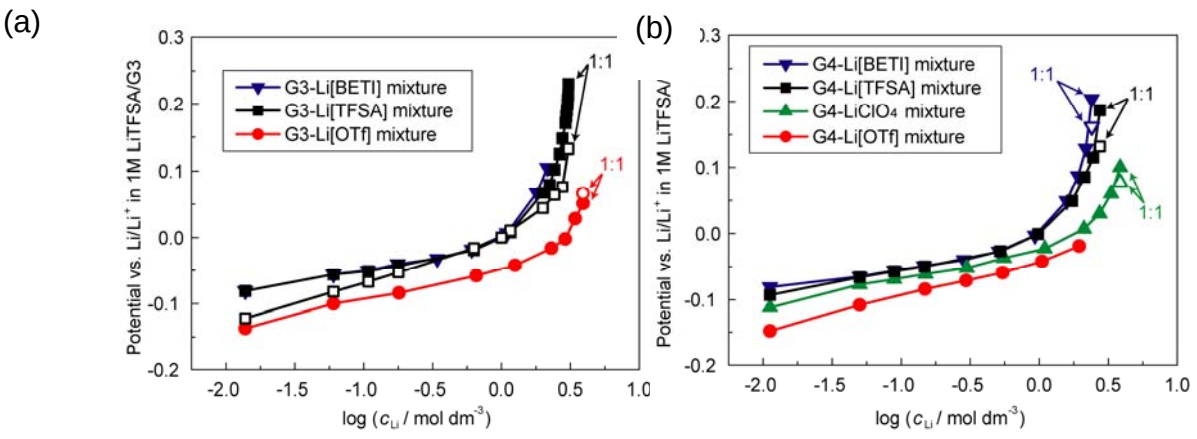

Figure 9. Plots of the Li/Li^+ electrode potential against common logarithm of the Li salt concentration in (a) G3-LiX mixtures and (b) G4-LiX mixtures at 30 °C. The reference electrode was Li/Li^+ in 1 mol dm^{-3} Li[TFSA]/G3. Open symbols represent the calculated electrode potential of Li/Li^+ on the basis of Eq. 6 and c_f obtained from the Raman spectroscopic analysis.

If the activity a_{Li+} is replaced by the concentration c_{Li}, Eq. 5 rationalizes the linear change in the potential against log c_{Li} in the dilute region below 1 mol dm^{-3}. However, the electrode potential exhibits non-linear increases at c_{Li} > 1 mol dm^{-3} (log c_{Li} > 0) for the other glyme-LiX mixtures, as well as the G3-Li[TFSA] mixtures. To interpret this remarkably high potential, we assumed a more detailed equilibrium reaction at the Li metal electrode, which takes into account the solvation/de-solvation processes of the glyme molecules: $[Li(glyme)]^+ + e^- \rightleftarrows Li + glyme$.[43] The electrode potential (E_2) can be written as:

$$E_2 = E_2^0 + \frac{2.303RT}{F} \log \frac{a_{[Li(glyme)_i]^+}}{a_{glyme}} \qquad (7)$$

where E_2^0 is the standard electrode potential, $a_{[Li(glyme)]+}$ and a_{glyme} are the activities of $[Li(glyme)]^+$ and free glyme, respectively. In this equation, the logarithm diverges to an infinitely high value if a_{glyme} was zero. In the concentrated regime where the amount of free glyme was very small, Eq. 7 is likely to account for the non-linear increase and the remarkably high electrode potential.

A study of the anionic dependence of the glyme-LiX mixtures revealed that the electrode potential was higher for more dissociative anions over the whole concentration range, and the order of the anions for the electrode potential is consistent with the order of the cation-anion (Li-X) interactions: [BETI] ~ [TFSA] > ClO_4 > [OTf]. At lower concentrations, the lower electrode potential for the glyme-Li[OTf] mixtures can be ascribed to the lower degree of dissociation of the Li salt (i.e. the low value of a_{Li+}). Indeed, the ionic conductivity of the G3-Li[OTf] mixtures was much lower than that of the G3-Li[TFSA] mixtures (**Figure S3**). The difference in the electrode potentials of the mixtures with dissociative and associative Li salts, is more pronounced at higher concentrations, probably due to the difference in both $a_{[Li(glyme)]+}$ and a_{glyme} as indicated by Eq. 7.

To examine the modified equilibrium reaction in the concentrated regime (c_{Li} > 1 mol dm^{-3}), the electrode potential E_2 was estimated using Eq. 7. Here $a_{[Li(glyme)]+}$ was assumed to be equal to c_{Li}, and a_{glyme} was substituted by c_f which was determined from the Raman spectroscopic analysis (previous section). In the dilute solutions (c_{Li} ≤ 1mol dm^{-3}), we also assume that $a_{[Li(glyme)]+} = c_{Li}$ and $a_{glyme} = c_G - c_{Li}$ for the calculation of E_2 using Eq. 7. The detailed procedure is described in the Supplementary Information. As

shown in **Figure 9**, the non-linear increase in the electrode potential at higher concentrations was demonstrated by the estimated E_2 for the G3-Li[TFSA] mixtures (open squares in **Figure 9a**). In addition, the estimated E_2 for [Li(glyme)]X with different anions explains the difference in the electrode potentials among [Li(glyme)]X. The agreement of the estimated E_2 with the experimental values indicates that the amount of free glyme is the crucial factor for the electrode potential of Li/Li^+ in the concentrated regime. Conversely, the fraction of free glyme in [Li(glyme)]X was estimated (**Table 1**) from the experimental E_2 values on the basis of Eq. S2, where the activities $a_{[Li(glyme)]+}$ and a_{glyme} were replaced by the corresponding concentrations and the 1mol dm^{-3} Li[TFSA]/G3 solution was defined as the reference. While we could not compare the exact values obtained from these two methods, the dependence of ionic structure on c_f/c_G was qualitatively consistent between the calculations, and we could conclude that free glyme scarcely exists in the solvate ILs (such as [Li(G3)][TFSA], [Li(G4)][TFSA] and [Li(G4)][BETI]).

Table. 1 The fraction of free glyme (c_f/c_G) in [Li(glyme)]X estimated by Raman spectroscopy and Li/Li^+ electrode potential.

	c_f/c_G (%) from Raman spectroscopy	c_f/c_G (%) from Li/Li^+ electrode potential
[Li(G3)][TFSA]	2.3	0.057
[Li(G3)][TfO]	30	53
[Li(G4)][BETI]	0.78	0.16
[Li(G4)][TFSA]	2.4	0.29
$[Li(G4)]ClO_4$	20	8.2

The electrode potential of Li/Li^+ in the solvate ILs containing an infinitesimal amount of free glymes (such as [Li(G3)][TFSA], [Li(G4)][TFSA], and [Li(G4)][BETI]), was significantly higher than the potential in the 1 mol dm^{-3} Li[TFSA]/G3 reference solution. This suggests that Li^+ (or $[Li(glyme)]^+$) is thermodynamically less stable in the solvate ILs than in the reference solution, even though the solvate ILs were found to be highly dissociated (i.e., high ionicity).[18] This specific Li^+ solvation environment in the solvate ILs could also be the difference from the concentrated solutions such as [Li(G3)][OTf].

4. CONCLUSIONS

In this study, we investigated the solvation of Li^+ in [Li(glyme)]X with different anionic structures, by Raman spectroscopy and ab initio molecular orbital calculations. While crystalline complexes of [Li(glyme)]X have various Li^+ coordination structures, including polymeric, dimeric, and monomeric complex cations, depending on the glyme and anionic structure, the crown-ether like $[Li(glyme)]^+$ complex cation was dominantly formed in the molten [Li(glyme)]X owing to a larger gain in the translational and rotational entropy upon melting. We estimated the concentration of the uncoordinated glymes in molten [Li(glyme)]X, which were generated through the equilibrium reaction LiX + glyme ⇄ $[Li(glyme)]^+ + X^-$. Only a very small amount of free glyme was discernible in the [Li(glyme)]X with [TFSA] or [BETI], and thereby they could be classified as solvate ILs. On the other hand, [Li(glyme)]X with other anions was found to contain >10 % of free glymes, and their percentages increased when combined with more associative anions. These results corroborate our previous categorization of [Li(glyme)]X into solvate ILs.[18] The X-ray structure factors indicated that CIP formation was more pronounced in [Li(G3)][TFSA] than in [Li(G4)][TFSA]. In addition, we demonstrated that the concentration of free glyme in [Li(glyme)]X influenced the electrode potential of Li/Li^+. The lower activity of free glyme (a_{glyme}) in the solvate ILs leads to a higher electrode potential (by about 200 mV) than that in the 1 mol dm^{-3} Li[TFSA] reference solution. This suggests that the Li^+ solvation environment is energetically more unstable in the solvate ILs despite the dissociation into $[Li(glyme)]^+$ and X^-. The frustrated Li^+ solvation, along with the low activity of free glyme are responsible for the specific electrode reactions in the solvate IL-based electrolytes for Li batteries such as graphite anode[43] and sulfur cathode.[44, 45]

ACKNOWLEDGMENT: This study was supported in part by the Advanced Low Carbon Technology Research and Development Program (ALCA) of the Japan Science and Technology Agency (JST), and by the Technology Research Grant Program of the New Energy and Industrial Technology Development Organization (NEDO) of Japan. The synchrotron radiation experiment was carried out with the approval of the Japan Synchrotron Radiation Research Institute (JASRI) (Proposal Nos. 2011A1373, 2012A1669, and 2012A1682). This work was partly supported by JSPS KAKENHI Grant Number 26-165, for which R. T. is grateful. The authors thank Dr. Wesley A. Henderson for his helpful discussions on Raman spectroscopy.

Supplementary Information: Deconvolution results of Raman spectra, normalized Raman spectra of glyme-Li salt mixtures, ionic conductivity of the G3-Li[TFSA] and G3-Li[OTf] mixtures, and the detailed procedure for calculating the electrode potential of Li/Li^+ (E_2).

References

1. K. Xu, *Chem. Rev.*, 2004, **104**, 4303-4418.
2. P. G. Bruce, S. A. Freunberger, L. J. Hardwick and J. M. Tarascon, *Nature Mater.*, 2012, **11**, 19-29.
3. C. P. Rhodes and R. Frech, *Macromolecules*, 2001, **34**, 2660-2666.
4. Y. G. Andreev, V. Seneviratne, M. Khan, W. A. Henderson, R. E. Frech and P. G. Bruce, *Chem. Mater.*, 2005, **17**, 767-772.
5. P. Johansson, J. Tegenfeldt and J. Lindgren, *Polymer*, 1999, **40**, 4399-4406.
6. A. G. Baboul, P. C. Redfern, A. Sutjianto and L. A. Curtiss, *J. Am. Chem. Soc.*, 1999, **121**, 7220-7227.
7. W. A. Henderson, N. R. Brooks, W. W. Brennessel and V. G. Young, *Chem. Mater.*, 2003, **15**, 4679-4684.
8. W. A. Henderson, N. R. Brooks and V. G. Young, *Chem. Mater.*, 2003, **15**, 4685-4690.
9. W. A. Henderson, F. McKenna, M. A. Khan, N. R. Brooks, V. G. Young and R. Frech, *Chem. Mater.*, 2005, **17**, 2284-2289.
10. C. Zhang, D. Ainsworth, Y. G. Andreev and P. G. Bruce, *J. Am. Chem. Soc.*, 2007, **129**, 8700-8701.
11. C. Zhang, Y. G. Andreev and P. G. Bruce, *Angew. Chem. Int. Ed.*, 2007, **46**, 2848-2850.
12. W. A. Henderson, *J. Phys. Chem. B*, 2006, **110**, 13177-13183.
13. T. M. Pappenfus, W. A. Henderson, B. B. Owens, K. R. Mann and W. H. Smyrl, *J. Electrochem. Soc.*, 2004, **151**, A209-A215.
14. T. Tamura, K. Yoshida, T. Hachida, M. Tsuchiya, M. Nakamura, Y. Kazue, N. Tachikawa, K. Dokko and M. Watanabe, *Chem. Lett.*, 2010, **39**, 753-755.
15. K. Yoshida, M. Nakamura, Y. Kazue, N. Tachikawa, S. Tsuzuki, S. Seki, K. Dokko and M. Watanabe, *J. Am. Chem. Soc.*, 2011, **133**, 13121-13129.
16. C. A. Angell, Y. Ansari and Z. Zhao, *Faraday Discuss.*, 2012, **154**, 9-27.
17. T. Mandai, K. Yoshida, K. Ueno, K. Dokko and M. Watanabe, *Phys. Chem. Chem. Phys.*, 2014, **16**, 8761-8772.
18. K. Ueno, K. Yoshida, M. Tsuchiya, N. Tachikawa, K. Dokko and M. Watanabe, *J. Phys. Chem. B*, 2012, **116**, 11323-11331.
19. B. L. Papke, M. A. Ratner and D. F. Shriver, *J. Electrochem. Soc.*, 1982, **129**, 1434-1438.
20. K. Yoshida, M. Tsuchiya, N. Tachikawa, K. Dokko and M. Watanabe, *J. Phys. Chem. C*, 2011, **115**, 18384-18394.
21. M. Isshiki, Y. Ohishi, S. Goto, K. Takeshita and T. Ishikawa, *Nucl. Instrum. Meth. A*, 2001, **467–468, Part 1**, 663-666.
22. S. Kohara, K. Suzuya, Y. Kashihara, N. Matsumoto, N. Umesaki and I. Sakai, *Nucl. Instrum. Meth. A*, 2001, **467–468, Part 2**, 1030-1033.
23. S. Sasaki, in *KEK Report* National Laboratory for High Energy Physics, Japan, 1991, vol. 90-16.
24. D. T. Cromer and J. B. Mann, *J. Chem. Phys.*, 1967, **47**, 1892-1893.
25. P. J. Brown, A. G. Fox, E. N. Maslen, M. A. O'Keefe and B. T. M. Willis, in *International Tables for Crystallography Volume C: Mathematical, physical and chemical tables*, ed. E. Prince, Springer Netherlands, 2004, vol. C, pp. 554-595.
26. G. Johanson and M. Sandstörm, *Chem. Scr.*, 1973, **4**, 195-198.
27. M. J. Frisch, G. W. Trucks, H. B. Schlegel, G. E. Scuseria, M. A. Robb, J. R. Cheeseman, G. Scalmani, V. Barone, B. Mennucci, G. A. Petersson, H. Nakatsuji, M. Caricato, X. Li, H. P. Hratchian, A. F. Izmaylov, J. Bloino, G. Zheng, J. L. Sonnenberg, M. Hada, M. Ehara, K. Toyota, R. Fukuda, J. Hasegawa, M. Ishida, T. Nakajima, Y. Honda, O. Kitao, H. Nakai, T. Vreven, J. A. Montgomery Jr., J. E. Peralta, F. Ogliaro, M. J. Bearpark, J. Heyd, E. N. Brothers, K. N. Kudin, V. N. Staroverov, R. Kobayashi, J. Normand, K. Raghavachari, A. P. Rendell, J. C. Burant, S. S.

Iyengar, J. Tomasi, M. Cossi, N. Rega, N. J. Millam, M. Klene, J. E. Knox, J. B. Cross, V. Bakken, C. Adamo, J. Jaramillo, R. Gomperts, R. E. Stratmann, O. Yazyev, A. J. Austin, R. Cammi, C. Pomelli, J. W. Ochterski, R. L. Martin, K. Morokuma, V. G. Zakrzewski, G. A. Voth, P. Salvador, J. J. Dannenberg, S. Dapprich, A. D. Daniels, Ö. Farkas, J. B. Foresman, J. V. Ortiz, J. Cioslowski and D. J. Fox, *Gaussian 09*, (2009) Gaussian, Inc., Wallingford, CT, USA.

28. D. M. Seo, P. D. Boyle, R. D. Sommer, J. S. Daubert, O. Borodin and W. A. Henderson, *J. Phys. Chem. B*, 2014, **118**, 13601-13608.
29. D. Brouillette, D. E. Irish, N. J. Taylor, G. Perron, M. Odziemkowski and J. E. Desnoyers, *Phys. Chem. Chem. Phys.*, 2002, **4**, 6063-6071.
30. X. Yang, Z. Su, D. Wu, S. L. Hsu and H. D. Stidham, *Macromolecules*, 1997, **30**, 3796-3802.
31. L. Ducasse, M. Dussauze, J. Grondin, J. C. Lassegues, C. Naudin and L. Servant, *Phys. Chem. Chem. Phys.*, 2003, **5**, 567-574.
32. J. Grondin, J.-C. Lassegues, M. Chami, L. Servant, D. Talaga and W. A. Henderson, *Phys. Chem. Chem. Phys.*, 2004, **6**, 4260-4267.
33. R. Frech and W. Huang, *Macromolecules*, 1995, **28**, 1246-1251.
34. H. Matsuura and K. Fukuhara, *J. Polym. Sci. B: Polym. Phys.*, 1986, **24**, 1383-1400.
35. P. Johansson, J. Grondin and J.-C. Lassègues, *J. Phys. Chem. A*, 2010, **114**, 10700-10705.
36. N. Dhuaml and S. Gejji, *Theor. Chem. Acc.*, 2006, **115**, 308-321.
37. S. Tsuzuki, W. Shinoda, S. Seki, Y. Umebayashi, K. Yoshida, K. Dokko and M. Watanabe, *ChemPhysChem*, 2013, **14**, 1993-2001.
38. Y. Umebayashi, T. Mitsugi, S. Fukuda, T. Fujimori, K. Fujii, R. Kanzaki, M. Takeuchi and S.-I. Ishiguro, *J. Phys. Chem. B*, 2007, **111**, 13028-13032.
39. M. Schmeisser, P. Illner, R. Puchta, A. Zahl and R. van Eldik, *Chem. Eur. J.*, 2012, **18**, 10969-10982.
40. P. Johansson, *Phys. Chem. Chem. Phys.*, 2007, **9**, 1493-1498.
41. S. Tsuzuki, W. Shinoda, M. Matsugami, Y. Umebayashi, K. Ueno, T. Mandai, S. Seki, K. Dokko and M. Watanabe, *Phys. Chem. Chem. Phys.*, 2015, **17**, 126-129.
42. R. H. Stokes and R. A. Robinson, *J. Am. Chem. Soc.*, 1948, **70**, 1870-1878.
43. H. Moon, R. Tatara, T. Mandai, K. Ueno, K. Yoshida, N. Tachikawa, T. Yasuda, K. Dokko and M. Watanabe, *J. Phys. Chem. C*, 2014, **118**, 20246-20256.
44. K. Dokko, N. Tachikawa, K. Yamauchi, M. Tsuchiya, A. Yamazaki, E. Takashima, J.-W. Park, K. Ueno, S. Seki, N. Serizawa and M. Watanabe, *J. Electrochem. Soc.*, 2013, **160**, A1304-A1310.
45. K. Ueno, J.-W. Park, A. Yamazaki, T. Mandai, N. Tachikawa, K. Dokko and M. Watanabe, *J. Phys. Chem. C*, 2013, **117**, 20509-20516.